NASA Technical Memorandum 87071

A Comparison of Electronic Heterodyne Moire Deflectometry and Electronic Heterodyne Holographic Interferometry for Flow Measurements

Arthur J. Decker and Josef Stricker
Lewis Research Center
Cleveland, Ohio

Prepared for the
Aerospace Technology Conference and Exposition
sponsored by the Society of Automotive Engineers
Long Beach, California, October 14–17, 1985

NASA

ABSTRACT

Electronic heterodyne moire deflectometry and electronic heterodyne holographic interferometry are compared as methods for the accurate measurement of refractive index and density change distributions of phase objects. Experimental results are presented to show that the two methods have comparable accuracy for measuring the first derivative of the interferometric fringe shift. The phase object for the measurements is a large crystal of KD*P, whose refractive index distribution can be changed accurately and repeatably for the comparison. Although the refractive index change causes only about one interferometric fringe shift over the entire crystal, the derivative shows considerable detail for the comparison. As electronic phase measurement methods, both methods are very accurate and are intrinsically compatible with computer controlled readout and data processing. Heterodyne moire is relatively inexpensive and has high variable sensitivity. Heterodyne holographic interferometry is better developed, and can be used with poor quality optical access to the experiment.

E-2643

IN THIS PAPER, electronic heterodyne moire deflectometry and electronic heterodyne holographic interferometry are compared for the accurate measurement of refractive index and density distributions of phase objects. The work, on which the comparison is based, was done at NASA Lewis Research Center as part of a program to study the possibilities of automated, precise fringe measurement systems for use in wind tunnels. The two techniques, compared in this report, also have other applications, such as structural analysis and heat transfer measurements.

The advantages of an electronic heterodyne method are accuracy, the ability to interpolate continuously between fringe maxima, and computer compatibility. In using an electronic heterodyne method, the relative phase between two points in a time varying fringe pattern is measured. This phase is then related to the difference in fringe number between the two points. Since phase measurements can be accomplished to better than a degree, fringe interpolation accuracies better than 1/360 fringe are possible.

Electronic heterodyne interferometry, holography, and holographic interferometry have been under development for more than a decade (1-6)*. A fringe-interpolation accuracy of 1/1000 of a fringe has been demonstrated by Dändliker in measuring the bending of a structure using electronic heterodyne holographic interferometry (2). Farrel, Springer, and Vest have used the technique to measure concentrations and temperatures of gas mixtures (5). A commercial multichannel electronic heterodyne interferometer is available (6), and the image dissector has been demonstrated for the rapid scanning and heterodyne measurement of a fringe pattern (3). The problem with using electronic heterodyne holography are those of holography itself: noise and nonlinearities. The method also requires interferometric stability for readout.

Deflectometry, whose best known representative is Toppler schlieren has recently been rediscovered to be quantitative as well as qualitative (7-10). Moire deflectometry allows both the magnitude and direction of a light-ray deflection to be measured. The application of the heterodyne readout technique to moire fringes is quite new (11-13), but it offers the same advantages to moire as to interferometry.

The relative states of development of electronic heterodyne moire and interferometry can be summarized. The measurement of fringes in electronic heterodyne holography and interferometry has been studied thoroughly, and

*Numbers in parentheses designate references at end of paper.

shot-noise limited accuracy has been claimed (2). Better methods for introducing a frequency difference between the two interfering beams are still being sought (14).

In contrast, the limitations on the performance of electronic heterodyne moire are still subjects for research and development. The fringe modulation method discussed in this report is simple to implement and offers ten times the interpolation accuracy of a measurement based on intensity. But the technique is highly anharmonic, and new fringe modulation techniques must be developed.

An obvious advantage of an electronic heterodyne method is its computer compatibility: the output of the measurement consists of electronically generated detector positions and phases. Another advantage is that an accurate derivative of the interferometer fringe number can be generated. Howes and Buchele (15) pointed out many years ago that, even when the two-dimensional approximation is used in interferometry, accounting for refraction effects requires an accurate knowledge of the first derivative of the fringe number. Howes has recently reemphasized this fact, while comparing rainbow schlieren (a form of deflectometry) with interferometry (10). Furthermore, if there is a large enough field of view that one can use computed tomography to calculate the density or density-change distribution from the fringes, the interferometer fringe differences and derivatives are required (16).

Holographic interferometry and moire deflectometry offer their own advantages for making these automated, precise measurements. Holographic interferometry offers its advanced stage of development, its compatibility with poor quality optics, and its ability to capture several perspectives or views of a time-varying flow field in a single hologram. Moire recording is less expensive than holography, is free from the holographic noise problem, has adjustable sensitivity, is directionally sensitive to density gradients, and is conceptually simple.

The precision of heterodyne holography and moire, which cannot be duplicated by other methods, suggests that the two be compared with one another. In this report, the comparison is done for a particularly suitable phase object, a so-called flow simulator (17-19). The flow simulator, an especially large transverse electrooptic modulator of KD*P, has the following advantages. The field of refractive-index-changes can be made precisely the same for moire and holography, allowing a meaningful comparison. The maximum change, over the entire crystal, can be restricted to less than one interferometer fringe shift, for a test of the relative precisions of moire and interferometry. Yet, in spite of the small total variation of fringe number, the derivative varies complexly, having extrema.

Before presenting the results of this comparison, diffuse-illumination holographic interferometry and moire deflectometry are reviewed briefly. Then heterodyne detection of both kinds of fringe patterns is explained and reviewed. The results of the comparison, using the flow simulator, are presented. Finally, the prospects for future development and applications of electronic heterodyne moire and electronic heterodyne holographic interferometry are summarized.

BACKGROUND - DIFFUSE-ILLUMINATION HOLOGRAPHIC INTERFEROMETRY

Diffuse-illumination holographic interferometry is well summarized in the book by Vest (20). The double-exposure method, the method reported herein, has been applied to wind-tunnel flows by many authors (21-26). The following summary contains the very essentials of diffusion-illumination, double-exposure holographic interferometry. The references should be consulted by anyone interested in a more comprehensive treatment.

If a double-exposure hologram is recorded of a diffusely illuminated flow field, where the density field of the flow changes between exposures, then the reconstructed image has the following properties. The fringes observed will definitely depend on the viewing or imaging system. If the reconstructed image of the doubly exposed flow field is viewed with a telecentric imaging system (an imaging system with constant perspective across the image), then the cosine fringe pattern is a parallel projection or Radon transformation of the density-change field, $\Delta\rho$.

That is, the fringe intensity varies according to $\cos \Delta\varphi$ where

$$\Delta\varphi = \frac{2\pi}{\lambda} G \int \Delta\rho \, ds \qquad (1)$$

and where the integrals are evaluated along lines parallel to the optical axis, extending from the imaged points, through the fluid, back to the diffuser. The coefficient G is the Gladstone-Dale coefficient, a function of the wavelength λ. At a wavelength of 532 nm, the wavelength of the second harmonic of the Nd:YAG laser,

$$G = 0.227 \times 10^{-3} \ m^3/kg$$

The interference fringes, however, are not imaged sharply for every plane in the flow field, as they would be for nondiffusion-illumination holographic interferometry. The fringes instead appear to be localized near surfaces or spatial curves. Only when the imaging system is focused near these curves or surfaces of localization do the fringes appear sharp or have high contrast.

When the surfaces or curves of localization can be simply related to a flow feature (for example, a shock wave surface), localization can be used as a flow visualization technique

(22-24). For quantitative work, however, it is desirable that the images of the fringes have a large depth of focus. Then, the placement or aperturing requirements of a detector used to measure the fringes are not critical. Fortunately, the depth of field and depth of focus can be enlarged, simply by increasing the F-number of the viewing or imaging system. An aperture greater than F/9 is not unreasonable.

The local visibility V of the fringe pattern, defined in terms of the local maximum and minimum intensities, I_{max} and I_{min}, by

$$V = \frac{I_{max} - I_{min}}{I_{max} + I_{min}} \tag{2}$$

and the local contrast C defined by

$$C = \frac{I_{max} - I_{min}}{I_{min}} \tag{3}$$

are affected by more than localization considerations. The hologram itself and the interferometric process are rich sources of noise, nonlinearities, and contrast reduction effects. All of these effects are discussed in detail in a paper on diffusion-illumination holographic interferometry in a flutter cascade (26). Speaking very briefly, a very good hologram might yield $C = 100$ and a bleached hologram might yield $C = 10$ to $C = 30$. The human eye might barely detect a contrast difference somewhere from $C = 0.1$ to $C = 1$. If care is not exercised, noise, nonlinear effects, and other contrast reduction effects can reduce the contrast to these minimum values, or less.

To minimize these effects, the hologram recording system must be designed to avoid extraneous reflections and to avoid recording other unused object information. The hologram must be recorded according to well published rules for holography, involving beam ratios, development procedures, coherence and polarization requirements, and beam geometries. The diffuser must be stable during the interexposure time; its transverse motion should be a fraction of the resolution of the final viewing system.

Finally, it must be stated that the above mentioned intensities are average intensities. It is assumed that detection occurs over a large number of speckles of the laser speckle effect. The signal to noise ratio, in the presence of laser speckle, improves as

$$(1 + N)^{1/2}$$

where N is the number of speckles within the detector aperture.

As is discussed next, moire has a very different description from holographic interferometry.

BACKGROUND - MOIRE DEFLECTOMETRY

A moire deflectometer consists of two identical Ronchi gratings (coarse rectangular-lined gratings), a collimated light source, and a diffusing screen, attached to the output grating. This arrangement is shown schematically in Fig. 1(a), together with a later-discussed arrangement for electronic heterodyne readout. The diffusing screen is used to view the fringe pattern, and is removed for electronic readout. The gratings are called G_1 and G_2 and are shown separated by a distance Δ.

Referring to Fig. 1(b), if the gratings are placed in contact, and if their lines are oriented at a small angle θ, then a pattern of moire fringes is easily observed. In the figure, the gratings of pitch (line separation) p are shown at angles $\theta/2$ and $-\theta/2$, respectively, relative to the y-axis. The moire fringes, light fringes where the grating lines intersect and dark fringes in between, are straight lines parallel to the x-axis and have a period p' given by (7)

$$\left[p' = \frac{p}{[2 \sin (\theta/2)]} \approx \frac{p}{\theta} \right] \tag{4}$$

Anyone interested in the subtleties of moire-fringe formation and moire-fringe contrast (9) should consult the references. Some essential facts can be stated briefly.

When the gratings are separated by a distance Δ, the separation between moire fringes is unaffected. However, unless

$$\Delta = n \frac{p^2}{\lambda} \tag{5}$$

where λ is the wavelength of light and n is an integer, the fringe contrast will decrease. When

$$\Delta = \left(n + \frac{1}{2} \right) \frac{p^2}{\lambda} \tag{6}$$

the fringes will vanish completely. A single wavelength is implied by these formulas. Collimated white light can be used to form moire fringes; however, the highest contrast fringes, over the largest range of grating separations Δ, are obtained by using the coherent illumination from a laser.

If the collimated light is refracted by a phase object before it enters the deflectometer, then the previously parallel moire fringes will be distorted. If a light ray, intersecting the gratings, has a component of refraction along the x-direction, then the fringe, where the light ray intersects the gratings, will shift position in the y-direction.

The angle φ_x of refraction from collimation is related to the fringe shift δh_y by the equation

$$\varphi_x = \theta \frac{\delta h_y}{\Delta} \tag{7}$$

Hence, by measuring δh_y as a function of position, then φ_x can be calculated as a function of position. Note that the sensitivity $\delta h_y/\varphi_x$ of the deflectometer can be adjusted by adjusting Δ and θ.

The refraction angle φ_x, in turn, is related to the x-direction derivative of refractive index, or density in the case of flows, by the equations

$$\varphi_x(x,y) = \frac{1}{n_f} \int_{Z_o}^{Z_f} \frac{\partial n}{\partial x}(x,y,z)\, dz \tag{8}$$

$$\varphi_x(x,y) = \frac{G}{n_f} \int_{Z_o}^{Z_f} \frac{\partial \rho}{\partial x}(x,y,z)\, dz \tag{9}$$

where Z_o and Z_f are the limits of the phase object along the line of sight and n_f is the refractive index of the medium surrounding the object. Note that these equations suppose that the distance-deflection of the light ray is negligible within the object. The distance-deflection between gratings is also neglected.

Recall from Eq. (1) for holographic interferometry, that the quantity measured in interferometry is proportional to

$$\int_{Z_o}^{Z_f} \Delta\rho(x,y,z)\, dz$$

If a flow versus no-flow comparison is performed, for example, then the data from interferometry must be differentiated once for comparison with the data of deflectometry.

The use of the electronic heterodyne method to measure fringe shifts or fringe number is discussed next.

ELECTRONIC HETERODYNE METHODS

INTERFEROMETRY - Electronic heterodyne interferometry can be defined and compared with ordinary interferometry by referring to the interference between two simple scaler waves

$$A \cos [\omega t + 2\pi f_a x]$$

and

$$B \cos [\omega t + 2\pi f_b x + \varphi]$$

where ω is the circular frequency of the light wave, and f_a and f_b are spatial frequencies.

The square-law detected interference between these two waves is given by

$$I = \frac{A^2}{2} + \frac{B^2}{2} + AB \cos [2\pi(f_b - f_a)x + \varphi] \tag{10}$$

The fringes are linear, unless the relative phase φ varies as a function of position. When $f_a \neq f_b$, the shift of a fringe maximum or minimum can be used to measure the x-variation of φ. The accuracy of this measurement is of the order of 10 percent of a fringe spacing. The accuracy is limited by the slow variation of I versus the phase near the extrema. Interpolation between extrema is not reliable for this reason, and because the variation of I with phase cannot be distinguished from the variation of I with A or B. However, the fringes can be photographed, and the centers of the bright fringes measured to better than 10 percent (15). Photographing the fringes precludes interpolation, however, because of the nonlinear response of the photographic emulsion.

Electronic heterodyne interferometry is not limited by these restrictions. In electronic heterodyne interferometry, the two waves have slightly different frequencies. For a difference of circular frequency $\Delta\omega$, the square-law detected interference between the waves is given by

$$I = \frac{A^2}{2} + \frac{B^2}{2} + AB \cos [\Delta\omega t + 2\pi(f_b - f_a)x + \varphi] \tag{11}$$

A linear detector placed anywhere in the pattern will output a signal proportional to

$$\cos [\Delta\omega t + 2\pi(f_b - f_a)x + \varphi]$$

independent of A and B. The phase of this signal can be measured relative to a reference with an accuracy better than 1° or better than 1/360 fringe.

This discussion applies to diffuse-illumination holographic interferometry, but there are complications.

DIFFUSE-ILLUMINATION, DOUBLE-EXPOSURE HOLOGRAPHIC INTERFEROMETRY - Electronic heterodyne, diffuse-illumination holographic interferometry has been well described by Dändliker (2,27). The complications alluded to above are associated with the holographic process, with diffusion-illumination interferometry, and with the phase measurement method.

A holographic setup for electronic heterodyne, diffuse-illumination holographic interferometry is shown schematically in Fig. 2(a), and a photograph of an actual setup is shown in Fig. 2(b). The subject for holography is a phase object, to be described in more detail later. The fringe imaging and readout

components are also shown in Fig. 2(a). The readout components are identical with those used for the moire technique, Fig. 1(a).

The holographic setup differs from that used to record an ordinary double-exposure hologram, only in that two distinct reference beams are used to record the hologram, one for each exposure. For a perfectly linear recording, each beam will reconstruct the image of the phase object, as it existed during the beam's own exposure. Each reference beam during reconstruction will also produce an extraneous wave from the other beam's hologram. But, if a large enough angle separates the two reference beams, these extraneous waves do not overlap with the reconstructed image of the phase object.

During the reconstruction process, a frequency difference is introduced between the two reference beams. This is accomplished by passing one of the two beams through an acoustooptic frequency shifter. The frequency shifter consists of two Bragg cells in series. When the hologram is recorded, the two cells are driven at the same frequency, and the diffraction order is selected where the frequency shifts introduced by the two cells cancel. During reconstruction, the two cells are driven at slightly different frequencies, and this frequency shift is imposed on the beam. The frequency difference used for this paper was 125 kHz. The interference pattern between the two reconstructed waves then varies at the frequency difference as in Eq. (11).

One complication is that the reference beam alignment must be exact during reconstruction; otherwise, a systematic phase error will be introduced. This phase error is mainly a linear variation of phase (2) or, equivalently, a constant shift of the first derivative. The error, should it occur, is minimized by placing the imaging lens as close to the hologram as possible. In diffuse illumination interferometry, proper realignment of the hologram is facilitated by maximizing the fringe contrast and by eliminating misalignment fringes that can be observed on the hologram, itself.

In addition to misalignment, another complication is the nonlinear response of the holographic emulsion. If Oa is the wave recorded by the first exposure, then the reconstructed wave will actually be given by

$$Oa + BaaOa + BabOb$$

where Ob is the wave recorded during the second exposure, and Baa and Bab are generally complex coefficients. Similarly, the wave reconstructed by the second reference wave is given by

$$Ob + BbbOb + BbaOa$$

The coefficients Bab and Bba in particular lead to positionally dependent phase errors. These coefficients can be minimized by controlling those holographic steps that improve linearity (exposure, beam ratio, processing) (28,29) and by eliminating from the hologram all object waves that do not ordinate from the changing part of the phase object.

Diffuse-illumination interferometry introduces complications not found in ordinary interferometry. As stated, the low frequency fringe pattern, containing information about the phase object, is determined in part by the imaging system. Each point in the fringe pattern is formed by a converging pencil of light rays. The pencil is determined, in turn, by the F-number of the imaging system; the pencil's cone angle decreases with increasing F. If high-contrast fringes are to be formed, the phase change, between exposure, must not vary over the pencil, at least to first order. That is, the fringe localization condition must be satisfied, or the F-number of the imaging system must be large to restrict the cone angle. For a symmetrical imaging system, the phase change is then associated with a central ray of the imaging system, and linear variations in phase, over the pencil of rays, will cancel. The fringes measured for this paper were imaged with an effective F/9.5 imaging system.

The laser speckle effect is the other complication of diffuse-illumination interferometry. The undesirable effect of speckle on a phase measurement is to introduce a speckle-to-speckle random phase change between the exposures of the double-exposure hologram. This random phase change is caused by interexposure transverse displacements, or apparent transverse displacements, of the diffuser. A displacement of the microstructure of the diffuser might be caused by vibration (in an actual wind tunnel), by a significant change in refraction between exposures, or by reference beam misalignment during the reconstruction process. Fortunately, the expected phase error can be reduced by averaging over many speckles; not nearly so many speckles are required as would be needed to achieve comparable accuracy with an intensity measuring system. According to Dändliker (2), the expected phase error is given by

$$\delta\varphi = [(1 - \gamma^2)/2\gamma^2(N + 1)]^{1/2} \qquad (12)$$

where

$$\gamma = \frac{2\,J_1\left(\frac{\pi S}{\lambda F}\right)}{\frac{\pi S}{\lambda F}}$$

and where F is the effective F-number (image distance divided by the lens diameter), N is the number of speckles within the detector aperture, and S is the transverse distance moved by the diffuser between exposures (or apparently moved by the diffuser between exposures). The coefficient γ is the fringe visibility (due

to motion of the diffuser alone). Sometimes, it is called the decorrelation coefficient.

The detectors used for this paper were 0.75 mm optical fibers routed to photomultiplier tubes. A 5.1 cm diameter lens was used to produce a magnification-unity image of the fringe pattern at a distance of 48.3 cm. The number of speckles, within the detector aperture, is given by

$$N = \frac{A_D A_L}{(\lambda d)^2}$$

where A_D is the detector area, A_L is the area of the lens pupil, and d is the image distance from the lens. Then, for the argon-ion laser used to record the holograms discussed herein

$$N = 1.5 \times 10^4$$

For γ greater than about 0.5, the phase error, due to the laser speckle effect, will be less than 1°.

The detection procedure itself introduces some complications. Two 0.75 mm fibers are used to read out the fringe pattern, one fixed and one movable. The fibers are connected to photomultiplier tubes. The output of the photomultiplier connected to the fixed fiber, after filtering and amplification, is fed to the reference input of a phase meter. The output of the photomultiplier connected to the movable fiber is fed to the signal input.

The reference is derived from the fringe pattern, rather than from a separate source, to introduce some common mode rejection into the measurements. Room air fluctuations and laser instabilities cause phase fluctuations. If equal phase shifts are introduced at both fibers, the phase difference is unaffected. Consequently, the output of the phase meter is observed to be much more stable, when the reference is generated by the fringe pattern.

The phase meter is capable of an accuracy of better than 1° or 1/360 fringe, but only if it is used carefully. The transfer function of the meter is nonlinear for phase differences approaching 180°, particularly for low signal to noise ratios. So, the meter's internal phase shifters are used to prevent more than a 90° reference-to-signal phase shift from occurring. Also, it is desirable that the signal level be kept as constant as possible.

The phase of the signal actually varies over the detector aperture. If the detector is symmetrical, and if the phase variation is approximately linear, then the output is the phase at the center of the detector.

Finally, it is to be noted that accurate detector positioning is essential, particularly if the results are to be differentiated. The maximum phase derivatives measured for this paper were about 10°/mm. Still, a positional accuracy better than 0.1 mm was necessary to realize the available accuracy.

Electronic heterodyne moire (Fig. 1(a)) uses exactly the same readout system as holography. However, the similarity ends there, as discussed next.

MOIRE DEFLECTOMETRY - As mentioned above, when the collimated light beam of the moire deflectometer is not disturbed by a phase object, the moire pattern consists of straight fringes parallel to the x-axis. An approximate expression for the intensity pattern of these fringes can be calculated from first principles (30,31). That expression is given by

$$I(y,\Delta^*) = \frac{1}{4} + \frac{2}{\pi^2} \sum_{m=0}^{\infty} \frac{\cos\left[\pi(2m+1)^2 \Delta^*\right]}{(2m+1)^2} \cos\left[2\pi(2m+1)\left(\frac{\chi}{p} + \frac{y\theta}{p}\right)\right] \qquad (13)$$

In this expression, $\Delta^* = \Delta/(p^2/\lambda)$ is the distance between the gratings in so-called Fourier units (Eq. (5)), and χ/p and $y\theta/p$ are phase shifts related to the relative translation and rotation of the Ronchi gratings. Here, χ is simply the x-directed offset between grating lines of the two gratings, and, as mentioned above, θ is the relative angle between grating lines. Note that the low-frequency moire fringe pattern is a consequence of the small value of θ. In fact, it is an assumption in deriving Eq. (13) that the variation of phase can be neglected over a distance p.

The basis of electronic heterodyne moire can be explained, if it is assumed that one grating, say G_2, is translated relative to the other at constant speed V in the x-direction. Then, the phase in Eq. (13) is replaced by the time varying phase

$$\psi(y,t) = \frac{\chi}{p} + \frac{y\theta}{p} + \frac{Vt}{p} \qquad (14)$$

and the intensity pattern of Eq. (13) is replaced by the time varying intensity pattern

$$I(y,\Delta^*,t) = \frac{1}{4} + \frac{2}{\pi^2} \sum_{m=0}^{\infty} \frac{\cos\left[\pi(2m+1)^2 \Delta^*\right]}{(2m+1)^2} \cos\left[2\pi(2m+1)\left(\frac{\chi}{p} + \frac{y\theta}{p} + \frac{\Omega}{2\pi} t\right)\right] \qquad (15)$$

with a fundamental frequency

$$\Omega = 2\pi V/p$$

If the higher harmonics are filtered out, then the signal is given by the expression

$$I_1(y,\Delta^*,t) = \frac{1}{4} + \frac{2}{\pi^2} \cos(\pi\Delta^*) \cos\left[2\pi\left(\frac{\chi}{p} + \frac{y\theta}{p} + \frac{\Omega t}{2\pi}\right)\right] \qquad (16)$$

The phase of this signal can be measured in the same way as explained for electronic heterodyne holographic interferometry.

The effect of refraction by a phase object is to introduce a phase shift

$$\Delta\psi = \frac{\varphi_x \Delta}{p} = \frac{\delta h_y}{p}$$

already discussed in connection with Eq. (7). A procedure for measuring this phase shift is to record the electronic phase, relative to that of a reference fiber as in holography, with and without the phase object. A flow versus no-flow condition would be an example. A point-by-point subtraction of the phases, with and without the phase object, then yields the phase shift as a function of position. Equations (7) to (9) are then used to compute the properties of the phase object.

The implication is that the above measurements are accomplished in real time. But, there is an alternative for rapidly changing phase objects (13). The shadow of gratings G_1 can be recorded on a glass photographic plate placed at the position of grating G_2. The distortions of the shadow of G_1, caused by the phase object, are thereby recorded for later readout. Readout is accomplished by placing the moving grating immediately in back of the processed photographic plate. When the combination is illuminated, a time varying signal is generated for phase measurement.

The state of development of electronic heterodyne moire is considerably more primitive than the state of development of electronic heterodyne diffuse-illumination holographic interferometry. At the time of writing of this paper, a technique for constant velocity movement of a grating was not perfected. As discussed later, the grating was moved sinusoidally by attaching it to an electromagnetic shaker. Possible sources of uncertainty in the measurements have not been evaluated to the same extent as for holography. There is a random error in using the phase meter. There will be an error, if the positions for the flow versus no-flow condition are not duplicated exactly. Moire is not affected by the speckle effect, but its signal, even for constant velocity motion of the grating, contains harmonics. There are other possible diffraction related effects due to the multitude of diffraction orders of the Ronchi gratings. These effects are being investigated.

The availability of electronic heterodyne holographic interferometry, to serve as a comparison, makes it possible to evaluate the actual performance of an electronic heterodyne moire deflectometer, in spite of these uncertainties. Another item that makes the evaluation meaningful is the availability of a phase object, whose properties can be duplicated exactly for holography and for moire. That phase object, a so-called gas-flow simulator, is discussed next.

MEASUREMENTS USING THE FLOW SIMULATOR

The flow simulator (17), based on a large crystal of KD*P, was originally constructed as a controllable phase object for testing holographic flow visualization systems (18,19). The crystal, Fig. 3, has 50 mm by 50 mm faces, which are perpendicular to the optic axis and are separated by 30 mm. Electrodes, 10 mm wide and 50 mm long, are attached to the 50 mm by 50 mm faces at 4 parallel edges.

The crystal is held in a mount, where it is submerged in Pockels cell fluid. Two parallel 30 mm by 50 mm faces are accessible through windows for allowing light to pass through the crystal. Light polarized perpendicular to the optic axis experiences refractive index changes, when voltages are applied to the electrodes. For this report, diagonally opposite electrodes 1 and 3 were grounded, and diagonally opposite electrodes 2 and 4 were raised to 5 kV to induce a refractive index change.

The holographic setup was the same as that employed by Weimer for the original evaluation of the flow simulator, except that two reference beams and an acoustooptic frequency shifter were added, as shown in Figs. 2(a) and 2(b). The crystal is diffusely illuminated from the back with horizontally polarized light. The 514.5 nm line of an argon-ion laser is used. One exposure is recorded with zero voltage on all electrodes. The other exposure is recorded with 5 kV applied to electrodes 2 and 4, as stated. In Fig. 4 is shown a photograph of the infinite fringe pattern corresponding to these conditions. When viewing the reconstructed image directly, it can be seen that the interference fringes are localized at midplane in the simulator, indicating that the transverse gradient of the refractive-index change is symmetrical about the midplane. The simulator was designed to simulate a two-dimensional flow.

In Fig. 5 is shown a comparison of the measurements made with the electronic heterodyne system with measurements made by Weimer (17). Both sets of measurements are for a horizontal scan midway between the two 50 mm by 50 mm faces. The electronic heterodyne interferometry was done for an infinite-fringe condition; whereas, Weimer used real-time, finite-fringe holographic interferometry, photographing the fringes for later measurement of the fringe shifts. The plot in Fig. 5 is of the fringe shift versus horizontal position measured from the left of the simulator. The fringe shift is assumed to be zero at midrange or $x = 25$ mm. The heterodyne results have been corrected to the wavelength of the HeNe laser at 632.8 nm, since this was the laser used by Weimer.

The two results compare very well, except near the upper left electrode. This is not surprising: the crystal near this electrode has shown deterioration since Weimer performed his measurements. It is interesting that the two measurements compare as well as they do, but

that confirms that the center of a photographed fringe can be located very accurately. The electronic heterodyne method is seen to yield a very smooth curve. The real test of the method is of its ability to yield accurate derivatives of the fringe shift, rather than the fringe shift itself.

For electronic heterodyne moire, Figs. 1(a) and 6, the crystal was illuminated by a collimated, horizontally polarized, HeNe laser beam, collimated by an off-axis parabolic mirror after having been diverged by a lens in front of the laser. The moire pattern was measured in real time, with and without voltage applied. As stated in the previous section, the two refraction fields were then subtracted to yield the refraction caused by the application of voltage.

There was a complication in using the moire deflectometer to make these measurements. The grating G_2 was vibrated sinusoidally, rather than moved at constant velocity. Vibration in the x-direction was accomplished by attaching the grating to an electromagnetic shaker. An analysis would require that Vt in Eq. (14) be replaced by the expression

$$A \sin \omega t$$

where ω is the shaker frequency and A is the shaker amplitude. A consequence was that the output of the electronic phase meter no longer varied linearly with the refraction angle. This complication was handled by means of a calibration procedure.

In order to minimize the nonlinear effect on the readout, the phase meter was gated such that the detector signal was blocked during half of the vibration cycle. A consequence was that measurements were made for one direction of grating travel only. The grating signal was generated by a square-wave signal generator (Fig. 1(a)).

The calibration procedure was as follows: while the grating was in motion and the reference detector was fixed at one position in the moire pattern (the calibration is sensitive to the reference-detector position), phase measurements using the test detector were recorded in the y-direction, in 20 μm steps. This measurement process was continued until the phase meter output had covered the meter's range of 360°, indicating that the optical fiber had moved a distance equal to a period of the moire fringe pattern. The calibration procedure was performed with the KD*P crystal in place, but with no voltage applied. The same calibration curve of phase versus displacement was measured with the crystal removed, indicating that removal of the crystal for calibration was not necessary. The detector was then returned to its original position, and the phase measured as a function of x. The calibration curve was then used to obtain δh_y of Eq. (7). The process was done with and without voltage, and the values of δh_y thereby measured were subtracted to measure the change in refraction.

The results of the holographic and moire measurements are compared in the next section.

RESULTS AND COMPARISON OF RESULTS

Before the results of electronic heterodyne interferometry and electronic heterodyne moire can be compared, the holographic data, Fig. 5, must be differentiated. The recording, differentiation, and error analysis of the holographic results are discussed next.

To record this data originally, the reference fiber was centered at $x = 2$ mm from the image of the left edge of the crystal. The interference fringes are localized at midplane in the crystal, making it possible to focus on the fringes and crystal simultaneously. The movable signal fiber was used to record the phase at stations separated by about 1 mm, beginning at $x = 5.6$ mm. A stepping motor translator with position indicator was used to position the signal fiber, but the position of this fiber was also checked using a laser interferometer. The translator and laser interferometer can be seen in the foreground of Fig. 2(b).

The derivative β' of the heterodyne interferometer phase is calculated from

$$\beta' = \frac{\beta_{i+G/2} - \beta_{i-G/2}}{x_{i+G/2} - x_{i-G/2}} \qquad °/\text{mm}$$

where G, the gauge length, an integer subscript, is approximately the distance over which the derivative is evaluated numerically. A value $G = 2$ or $x_{i+G/2} - x_{i-G/2} \approx 2$ mm was selected.

If the phase measurement has a random error $\delta\beta$, then the uncertainty $\delta\beta'$ of the derivative is given by

$$\delta\beta' = \frac{\sqrt{2}\,\delta\beta}{G}$$

For comparison with moire, the derivative of phase is converted to a derivative of refractive index. For that conversion, the two-dimensional approximation is assumed. In the two-dimensional approximation, Eq. (1) becomes

$$\Delta\eta_x = G\,\Delta\rho = \frac{\lambda\Delta\varphi}{2\pi(Z_f - Z_o)}$$

where η is the refractive index and $Z_f - Z_o$ is the extent of the phase object along the view. Then, the derivative of the change in refractive index is given by

$$\Delta\eta_x' = \frac{\lambda}{360L}\,\beta'$$

where L is the length of the crystal and the meter phase derivative in °/mm has been substituted. For the flow simulator L = 50 mm and $\lambda = 0.5145\times10^{-3}$ mm, so

$$\Delta\eta_i' = 0.2858\times10^{-6}\,\beta_i' \quad cm^{-1}$$

For quick reference, the maximum value of the phase derivative was

$$\beta' = 13.29°/mm$$

and the phase uncertainty had an absolute range $\delta\beta = 1°$ so

$$\delta\beta' = 0.7°/mm$$

Then

$$\Delta\eta'_{max} = 3.8\times10^{-6}/cm$$

and

$$\delta\Delta\eta' = 0.2\times10^{-6}/cm$$

A complete plot of the derivative of the change in refractive index versus position is shown for heterodyne holographic interferometry in Fig. 7(a).

There are some additional sources of error that affect Fig. 7(a). A telecentric imaging system was not used to image the fringe pattern; hence, the angle of the central ray varies across the crystal. The imaging lens was centered on the crystal. For the data shown, the central ray deviates from perpendicular at the windown by at most 2.3° on the left and 2.6° on the right. The effect, to first order, is a -1 mm positioning error at the ends of the travel of the signal fiber.

There are two errors introduced by the nonzero gauge length. For the features (extrema) shown in Fig. 7(a), there is a negligible magnitude error. But there is a positional uncertainty equal to the gauge length G: all feature positions are uncertain to ±1 mm.

It is estimated that the center line of the crystal was located within ±0.5 mm. Scans were also performed 1 mm above and 1 mm below the center scan. From these scans, it is determined that the positions of the extrema are not affected by the centerline uncertainty, but the heights of the extrema are affected. The effect is to double the error shown in Fig. 7(a).

These uncertainties and errors are to be kept in mind when comparing Fig. 7(a) with (b) showing the same results for electronic heterodyne moire.

There was no need to differentiate the results of the moire measurements. The change in δh_y between voltage and no-voltage states was substituted in Eq. (7) for the refraction angle φ_x. The two-dimensional approximation was asserted, and the refraction angle substituted in Eq. (8) to calculate the derivative of the change in refractive index.

The following parameters characterized the readout system used for the moire measurements. The phase measurement system was the same system used for holography. The separation between the Ronchi gratings was given by Δ = 32 cm. The pitch of the rulings was given by p = 0.17 mm, and the angle between rulings was selected to yield a fringe spacing of p' = 4.36 mm. That fringe spacing corresponded to an angle between rulings given by $\theta = 2.23°$.

As with holography, the data was recorded about every millimeter, and exact positions were determined using the interferometer. As with holography, the data scan was made along the center line. The position x from the left edge of the flow simulator ranged from 2 to 48 mm.

The error in positioning the detectors was the same as that of holography. The random error in using the phase meter was ±1° for a total random error for the two-phase measurements at each point of ±1.4°. The calibration curve and Eqs. (7) and (8) are used to calculate the error range shown in Fig. 7(b).

The two figures, 7(a) and (b), are plotted with the same coordinates. The figures show that, within the uncertainties mentioned above, the results of electronic heterodyne moire and electronic heterodyne holographic interferometry are the same. In particular, the same peaks or extrema appear in both figures.

CONCLUSIONS AND CONCLUDING REMARKS

In the previous section, electronic heterodyne moire deflectometry and electronic heterodyne, diffuse-illumination holographic interferometry were observed to compare favorably. The subject for measurement, a crystal of KD*P, corresponded to a weak flow object, yet the techniques showed considerable detail, detail not observable using ordinary intensity interferometry or deflectometry.

The present status is that electronic heterodyne holographic interferometry is quite suitable for development for applications. And some additional applications in a wind tunnel environment would be desirable to show how to design and to use this kind of interferometer. Nevertheless, it is clear that the reference beam optics, and also the object illumination, must be designed very carefully. Otherwise, excessive noise levels and systematic errors will occur. At the NASA Lewis Research Center, the approach is to combine the reference wave setup and the hologram magazine in a single transportable unit, to be moved back and forth between test rig and readout station.

Electronic heterodyne moire requires continuing development and analysis of the technique itself. The sinusoidal motion of the Ronchi grating in readout is undesirable, because of the need for a calibration procedure. A sawtooth ramping of the grating is being

investigated. Then, except during flyback, the moire-fringe crossing frequency will be a constant. Still, it would be desirable to have other than an electromechanical fringe modulation method. The objective would be to have an electronic Ronchi grating. Techniques being considered, among others, are liquid crystal arrays and polarization fringes.

Still, electronic heterodyne moire offers so many advantages that its continued development is worth the effort. Moire is not affected by the noise sources, nonlinearities, speckle problems, stability requirements, fixed sensitivity, and cost of electronic heterodyne holographic interferometry. The sensitivity of moire is adjustable.

Both techniques compared in this paper require procedures for processing large quantities of data effectively and sensibly. Both techniques promise to be useful and convenient-to-use instrument systems, but additional development, engineering and practice will be required.

REFERENCES

1. R. Crane, "Interference Phase Measurement," Applied Optics, Vol. 8, No. 3, Mar. 1969, pp. 538-542.
2. R. Dändliker, "Heterodyne Holographic Interferometry," in Progress in Optics, Vol. 17, E. Wolf, Ed., North-Holland Publishing Co., New York, 1980, pp. 1-84.
3. F.L. Merat, and P.C. Claspy, "Electronic Heterodyne Recording of Interference Patterns," in Interferometry; Proceedings of the Seminar, G.W. Hopkins, Ed., Society of Photo-Optical Instrumentation Engineers, Bellingham, WA, 1979, pp. 159-164.
4. A.J. Decker, Y.-H Pao, and P.C. Claspy, "Electronic Heterodyne Recording and Processing of Optical Holograms Using Phase Modulated Reference Waves," Applied Optics, Vol. 17, No. 6, Mar. 15, 1978, pp. 917-921.
5. P.V. Farrell, G.S. Springer, and C.M. Vest, "Heterodyne Holographic Interferometry: Concentration and Temperature Measurements in Gas Mixtures," Applied Optics, Vol. 21, No. 9, May 1, 1982, pp. 1624-1627.
6. N.A. Massie, M. Dunn, D. Swain, S. Muenter, and J. Morris, "Measuring Laser Flow Fields with a 64-Channel Heterodyne Interferometer," Applied Optics, Vol. 22, No. 14, July 15, 1983, pp. 2141-2151.
7. O. Kafri, "Noncoherent Method for Mapping Phase Objects," Optics Letters, Vol. 5, No. 12, Dec. 1980, pp. 555-557.
8. J. Stricker, and O. Kafri, "A New Method for Density Gradient Measurements in Compressible Flows," AIAA Journal, Vol. 20, No. 6, June 1982, pp. 820-823.
9. E. Bar-Ziv, S. Sgulim, O. Kafri, and E. Keren, "Temperature Mapping in Flames by Moire Deflectometry," Applied Optics, Vol. 22, No. 5, Mar. 1, 1983, pp. 698-705.
10. W.L. Howes, "Rainbow Schlieren Vs. Mach-Zehnder Interferometer: A Comparison," Applied Optics, Vol. 24, No. 6, Mar. 15, 1985, pp. 816-822.
11. J. Stricker, "Electronic Heterodyne Readout of Fringes in Moire Deflectometry," Optics Letters, Vol. 10, No. 6, June 1985, pp. 247-249.
12. G. Indebetouw, "Profile Measurements Using Projection of Running Fringes," Applied Optics, Vol. 17, No. 18, Sept. 15, 1978, pp. 2930-2933.
13. J. Stricker, "Moire Deflectometry With Deferred Electronic Heterodyne Readout," Applied Optics (To be published, Vol. 24, Aug. 1985).
14. K. Tatsuno, and Y. Tsunoda, "Diode Laser Heterodyne Interferometer Using Direct Modulation of Wavelength," presented at Conference on Lasers and Electro-Optics, Baltimore, May 1985 (OSA, New York, 1985).
15. W.L. Howes, and D.R. Buchele, "A Theory and Method for Applying Interferometry to the Measurement of Certain Two-Dimensional Gaseous Density Fields," NACA TN-2693, 1952.
16. S.R Deans, "The Radon Transform and Some of its Applications," Wiley, New York, 1983.
17. D. Weimer, "Pockels-Effect Cell for Gas-Flow Simulation," NASA TP-2007, 1982.
18. A.J. Decker, "Holographic Cinematography of Time-Varying Reflecting and Time-Varying Phase Objects Using a Nd:YAG Laser," Optics Letters, Vol. 7, No. 3, Mar. 1982, pp. 122-123.
19. A.J. Decker, "Measurement of Fluid Properties Using Rapid-Doubld-Exposure and Time-Average Holographic Interferometry," AIAA Paper 84-1461, June 1984.
20. C.M. Vest, "Holographic Interferometry," Wiley, New York, 1979.
21. J.D. Trolinger, "Flow Visualization Holographic," Optical Engineering, Vol. 14, No. 5, Sept.-Oct. 1975, pp. 470-481.
22. R.F. Wuerker, R.J. Kobayashi, L.O. Heflinger, and T.C. Ware, "Application of Holography to Flow Visualization Within Rotating Compressor Blade Row," AiResearch Manufacturing Co., Los Angeles, CA, Report AIRESEARCH-73-9489, Feb. 1984. (NASA CR-121264.)
23. A.J. Decker, "Fringe Localization Requirements for Three-Dimensional Flow Visualization of Shock Waves in Diffuse-Illumination, Double-Pulse Holographic Interferometry," NASA TP-1868, 1982.
24. A.J. Decker, "Holographic Flow Visualization of Time-Varying Shock Waves," Applied Optics, Vol. 20, No. 18, Sept. 15, 1981, pp. 3120-3127.
25. B. Carrigan, "Holographic Flow Visualization," National Technical Information Service, PB-808199, Apr. 1980.

26. A.J. Decker, "Evaluation of Diffuse-Illumination Holographic Cinematography in a Flutter Cascade," NASA TP (to be published).
27. R. Dändliker, B. Ineichen, B. Eliasson, J. Mastner, "Quantitative Strain and Stress Determination from Holographic Interferograms," Brown Boveri Research Center, Baden, Switzerland, Sept. 1977. (AD-A048640.)
28. R.J. Collier, C.B. Burckhardt, and L.H. Lin, "Optical Holography," Academic Press, New York, 1971.
29. H.J. Caulfield, ed., "Handbook of Optical Holography," Academic Press, New York, 1979.
30. E. Keren and O. Kafri, "Diffraction Effects in Moire Deflectometry," Journal of the Optical Society of America, Part A, Vol. 2, No. 2, Feb 1985, pp. 111-120.
31. E. Bar-Ziv, "Effect of Diffraction on the Moire Image. I-Theory," Journal of the Optical Society of America, Part A, Vol. 2, No. 3, Mar. 1985, pp. 371-379.

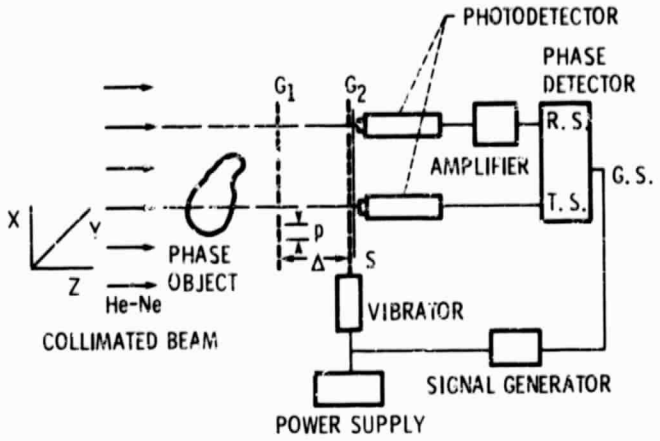

(a) Schematic of moire deflectometer with electronic heterodyne readout.

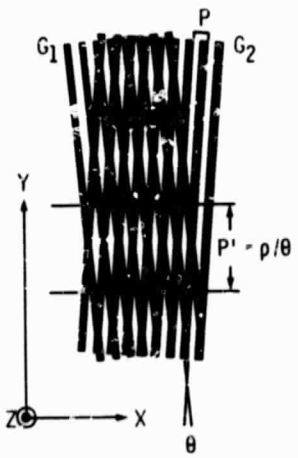

(b) Moire fringe pattern formed by Ronchi gratings.

Figure 1. - Moire deflectometry.

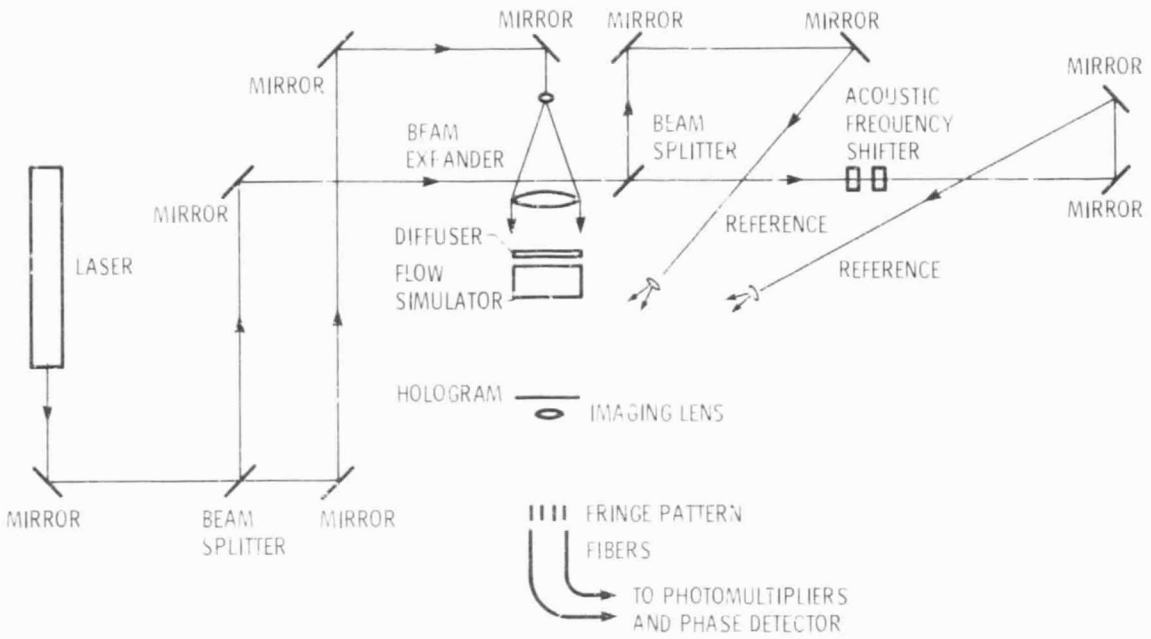

(a) Schematic.

Figure 2. - Electronic heterodyne holographic interferometer.

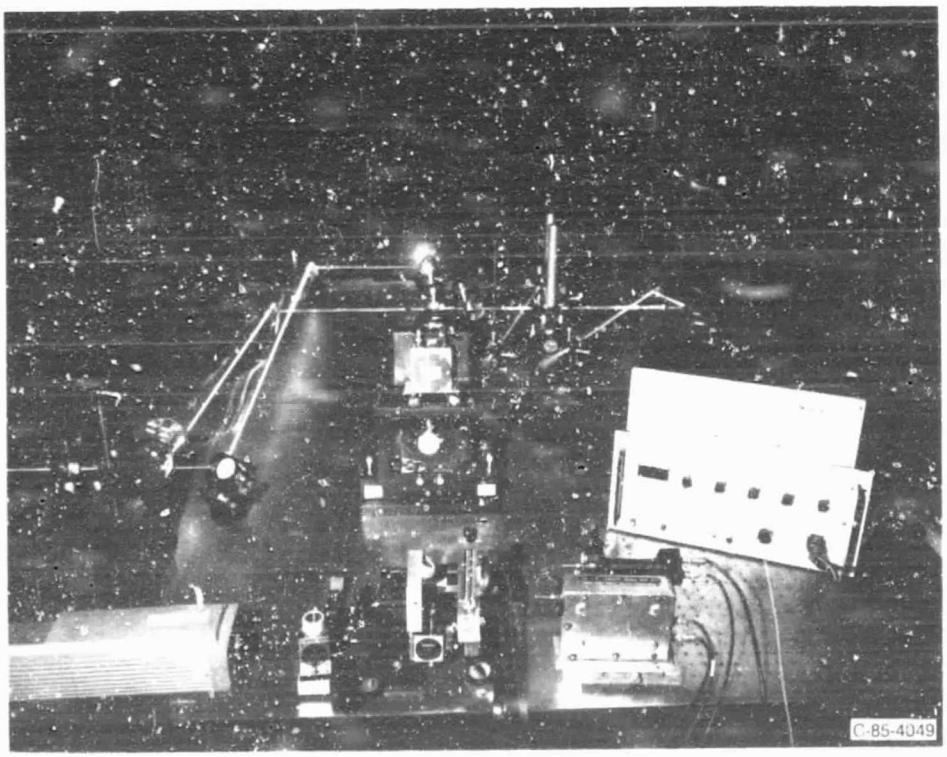

(b) Photograph of electronic heterodyne holographic interferometer.

Figure 2. - Concluded.

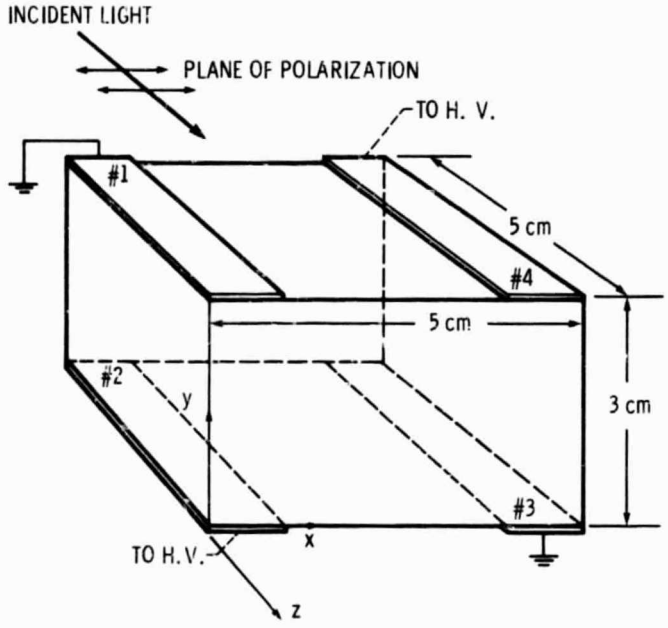

Figure 3. - Flow simulator-crystal of KD*P.

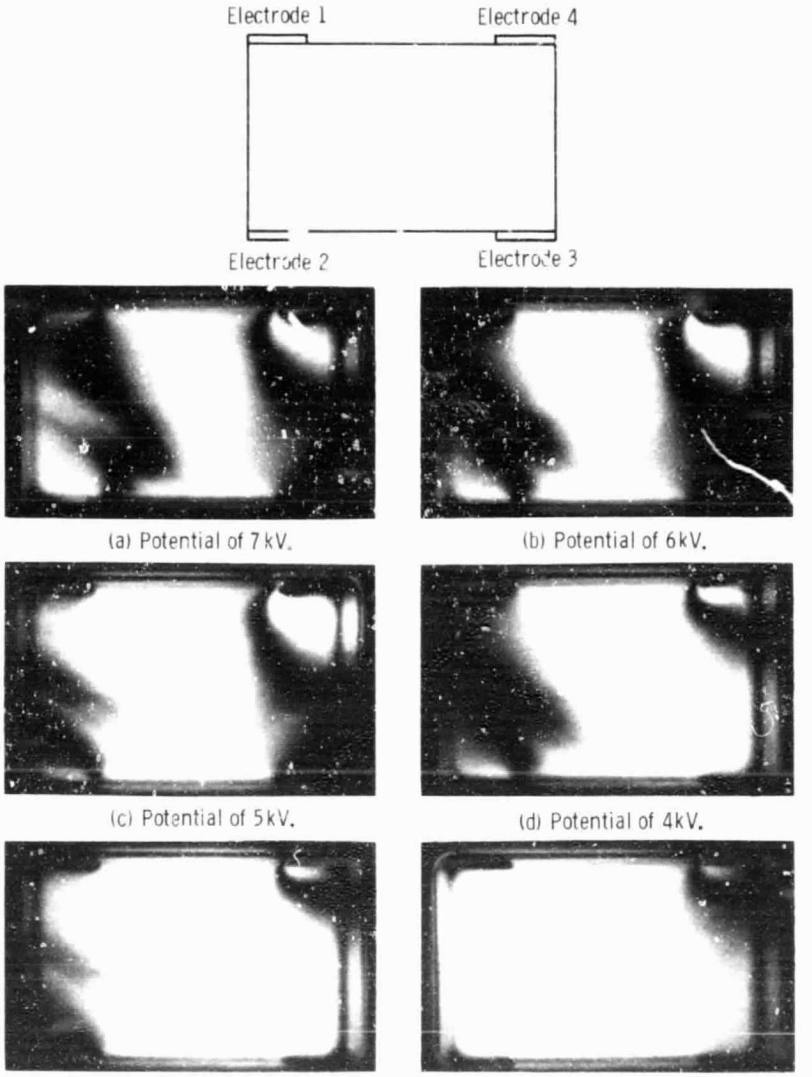

(a) Potential of 7 kV.

(b) Potential of 6kV.

(c) Potential of 5kV.

(d) Potential of 4kV.

(e) Potential of 3kV.

(f) Potential of 2kV.

Figure 4. - Infinite fringe patterns--Pockels flow simulator.

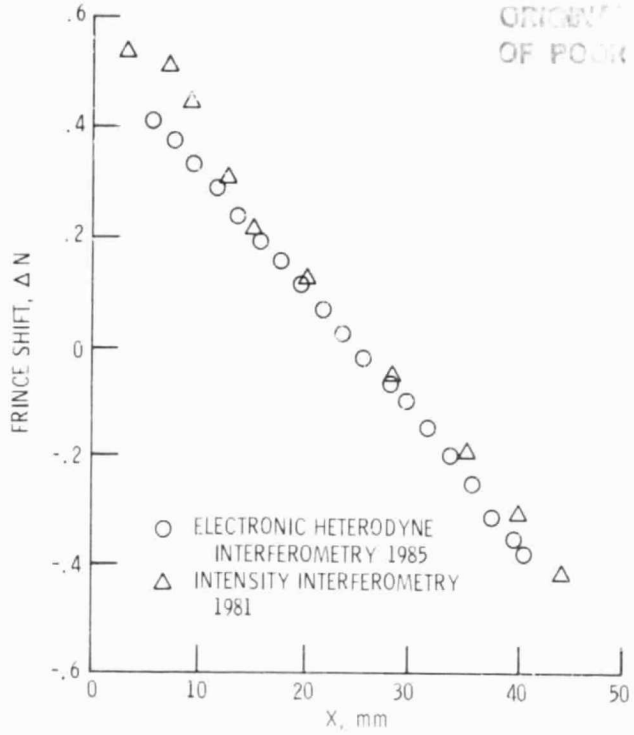

Figure 5. - Comparison of electronic heterodyne interferometry with intensity interferometry of flow simulator.

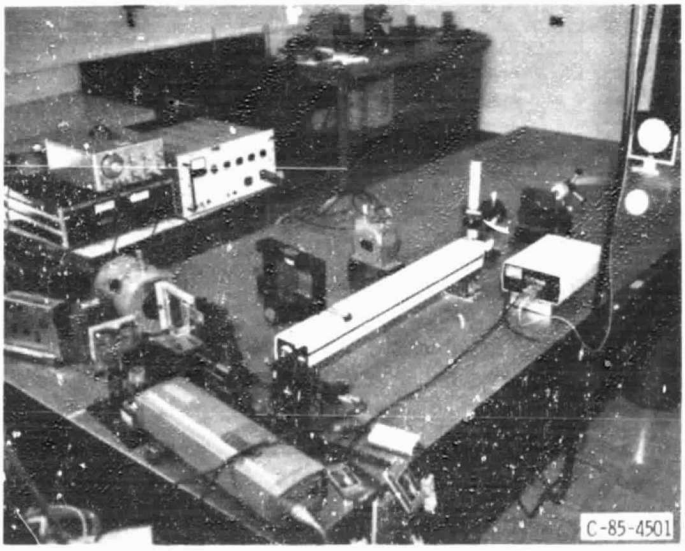

Figure 6. - Photograph of electronic heterodyne moire deflectometer.

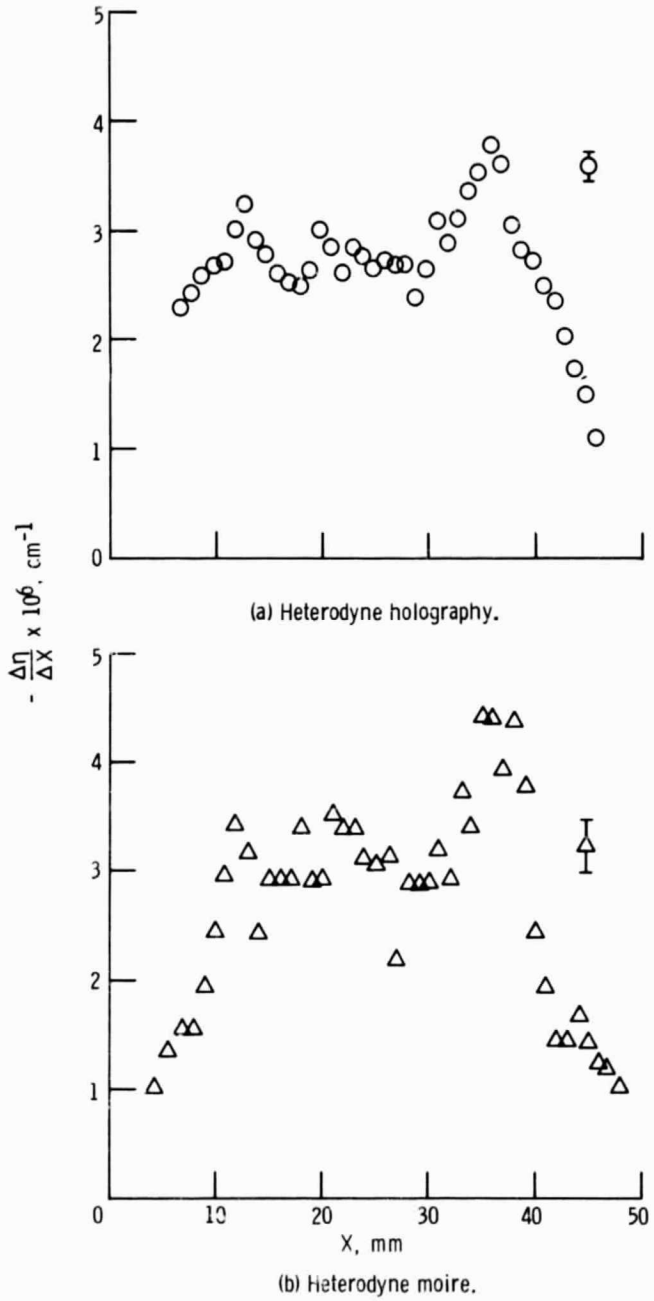

(a) Heterodyne holography.

(b) Heterodyne moire.

Figure 7. - X-derivative of refractive index for flow simulator.

1. Report No.	2. Government Accession No.	3. Recipient's Catalog No.
NASA TM-87071		

4. Title and Subtitle	5. Report Date
A Comparison of Electronic Heterodyne Moire Deflectometry and Electronic Heterodyne Holographic Interferometry for Flow Measurements	6. Performing Organization Code: 505-40-14

7. Author(s)	8. Performing Organization Report No.
Arthur J. Decker and Josef Stricker	E-2643
	10. Work Unit No.

9. Performing Organization Name and Address	11. Contract or Grant No.
National Aeronautics and Space Administration Lewis Research Center Cleveland, Ohio 44135	13. Type of Report and Period Covered: Technical Memorandum
12. Sponsoring Agency Name and Address	14. Sponsoring Agency Code
National Aeronautics and Space Administration Washington, D.C. 20546	

15. Supplementary Notes

Arthur J. Decker, Lewis Research Center; Josef Stricker, NRC-NASA Research Associate, on leave from Technion - Israel Institute of Technology, Haifa, Israel 32000. Prepared for the Aerospace Technology Conference and Exposition, sponsored by the Society of Automotive Engineers, Long Beach, California, October 14-17, 1985.

16. Abstract

Electronic heterodyne moire deflectometry and electronic heterodyne holographic interferometry are compared as methods for the accurate measurement of refractive index and density change distributions of phase objects. Experimental results are presented to show that the two methods have comparable accuracy for measuring the first derivative of the interferometric fringe shift. The phase object for the measurements is a large crystal of KD*P, whose refractive index distribution can be changed accurately and repeatably for the comparison. Although the refractive index change causes only about one interferometric fringe shift over the entire crystal, the derivative shows considerable detail for the comparison. As electronic phase measurement methods, both methods are very accurate and are intrinsically compatible with computer controlled readout and data processing. Heterodyne moire is relatively inexpensive and has high variable sensitivity. Heterodyne holographic interferometry is better developed, and can be used with poor quality optical access to the experiment.

17. Key Words (Suggested by Author(s))	18. Distribution Statement
Holography; Holographic interferometry; Moire deflectometry; Heterodyning	Unclassified - unlimited STAR Category 35

19. Security Classif. (of this report)	20. Security Classif. (of this page)	21. No. of pages	22. Price*
Unclassified	Unclassified		

*For sale by the National Technical Information Service, Springfield, Virginia 22161